Fuel 409 (2026) 137695

Contents lists available at ScienceDirect

Fuel

journal homepage: www.elsevier.com/locate/fuel

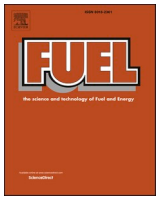

Full Length Article

Effect of ammonia on soot volume fraction and morphology in laminar flames: modeling the impact of NH_2 radicals☆

P. Crepaldi [a], A. Nobili [b], T. Dinelli [a], L. Pratali Maffei [a], A. Cuoci [a], T. Faravelli [a,*]

[a] CRECK Modeling Lab, Department of Chemistry, Materials, and Chemical Engineering "G. Natta", Politecnico di Milano, P.zza Leonardo da Vinci 32, Milano 20133, Italy
[b] Department of Mechanical Engineering, Stanford University, Stanford, CA 94305, United States

ARTICLE INFO

Keywords:
Ammonia
Carbonaceous nanoparticles
Flames
Kinetics

ABSTRACT

There is a growing scientific and industrial interest in ammonia as a zero-carbon fuel. This study examines the impact of ammonia on the reduction of soot formation in ethylene laminar flames using a comprehensive kinetic model. The study examines the influence of the NH_2 radical by incorporating its interaction with gas-phase aromatic species and soot particles into the adopted model. In this context, reference reaction rates are proposed and discussed. The model is compared to a set of experimental measurements of different target quantities, including soot volume fraction, f_v, in two distinct sets of counterflow flames. The model has been demonstrated to effectively predict pivotal morphological soot characteristics, including the progression of the average particle size (*D63*) in counterflow flames and the particle size distribution (PSD) in premixed burner-stabilized stagnation flames at a height above the burner, H_p, equals to 5 mm for diverse NH_3 concentrations. Nevertheless, it has been demonstrated that the model poorly predicts the bimodal distribution of the *PSD* when ammonia is introduced together with ethylene at $H_p = 10$ mm. Kinetic analyses are conducted to identify the primary competing reactions between N-containing species and hydrocarbons, which influence the observed and simulated reduction in 4-ring PAH in the presence of NH_3 relatively to pure ethylene flames. It is essential that future experimental studies be conducted to quantify N-containing hydrocarbons in laminar flames. This will serve to validate the findings of the kinetic modeling study and refine the understanding of pathways controlling soot chemistry in ammonia-doped flames.

1. Introduction

Ammonia (NH_3) is a key-player in the ongoing energy transition. Scientific interest in ammonia has grown markedly in recent years due to its high energy density, ease of transportation, and carbon-free nature, making it an attractive energy vector [1]. On the other hand, there are intrinsic limitations in the combustion characteristics of ammonia which restrict its application in energy generation system as pure fuel, e.g., low heating value, low laminar burning velocity and high auto-ignition temperature [2]. Therefore, blending ammonia with hydrocarbon fuels has emerged as an effective strategy to enhance combustion stability and reducing carbon emissions [3,4]. Hydrocarbon combustion is known to produce carbonaceous nanoparticles, or soot, which adversely affect both climate change and human health [5,6]. In this regard, it is largely proven that ammonia has a beneficial effect when mixed to traditional hydrocarbon fuels by drastically reducing soot emissions even at relatively low NH_3 content. These evidence raises the question on the fundamental mechanism through which ammonia drives soot suppression.

Many previous experimental studies quantitatively investigated sooting behavior in co-fired flames with ammonia. Bennett et al. [7] and Zhou et al. [8] experimentally described soot formation in ammonia/ethylene laminar counterflow flames, showing that soot volume fraction, f_v, peak can be reduced by about 87 % for a 20 % ammonia substitution to ethylene [8]. Shao et al. [9] confirmed soot reduction in ammonia/ethylene laminar premixed burner-stabilized stagnation flames. Steinmetz et al. [10] and Liu et al. [11] assessed similar impact of ammonia addition and substitution in ethylene co-flow flames. Different reaction pathways have been explored in the attempt to numerically predict PAH and soot reduction in ammonia doped

☆ This article is part of a special issue entitled: 'MCS13' published in Fuel.

* Corresponding author.
E-mail address: tiziano.faravelli@polimi.it (T. Faravelli).

https://doi.org/10.1016/j.fuel.2025.137695
Received 30 October 2025; Accepted 23 November 2025
Available online 2 December 2025

hydrocarbon flames. With respect to the core chemistry, it was observed that the interactions between ammonia and methane primary decomposition products result in a decrease in the concentration of C_2H_2, a key intermediate in the formation of benzene as well as in the growth of larger PAH [12]. Similarly, the addition of NH_3 reduced the concentration of propargyl radical (C_3H_3) [13], whose self-combination represents a major pathway towards benzene formation under flame conditions. More in detail, amino radical (NH_2) reaction with propargyl was estimated to be the major responsible for reducing pyrene concentration in both premixed and diffusion ammonia/ethylene flames with HCN and C_3H_3 interactions playing a minor role [13]. Additionally, N-containing compounds can also directly interact with aromatic species, hampering their growth towards soot. This phenomenon has been studied theoretically by Wang et al. [13], who explored the impact of HCN addition onto aromatics. They concluded that this pathway can temporarily block reactive sites and prevent further PAH growth through HACA mechanism. Liu et al. [11] computed similar reaction rate constants for HCN-PAH and C_2H_2 [11] at flame-relevant conditions, assuming the formation of aromatic species having saturated N-atoms in a heterocycle ring or in R-CN functional groups. On the other hand, Tang et al. [14] performed the simulation of a series of counterflow flames of C_2H_4/NH_3 from Zhou et al. [8], by including the reaction pathways for HCN-benzene and HCN-naphthalene theoretically explored [15]. The authors found a minor role played by HCN addition onto small aromatic species in suppressing larger PAH growth. Conversely, they identified, $C_2H_2 + N <=> HCN + CH$ as the main responsible in reducing acetylene formation. It is important to underline that this variety of pathways suggested in the recent literature as responsible of soot reduction in NH_3-doped flames primarily arises from the use of different core mechanisms to conduct the simulations. Moreover, model validation is typically performed on a limited amount of data, since literature measurements of soot, PAHs, N-containing aromatic and small hydrocarbon species are scarce.

Finally, it was observed that ammonia not only reduces soot formation in NH_3-doped flames, but it also affects particle morphology and nanostructure. Indeed, soot formed in NH_3-doped flames have lower particle average diameter [8] and primary particle diameter [16] as well as a different shape of particle size distribution [9] with respect to pure C_2H_4 flames. Furthermore, soot particles formed in the presence of ammonia show a more disordered structure, with shorter fringe length and higher tortuosity and inter-fringe spacing [16].

While much of the literature has emphasized gas-phase reactions between N-containing species and PAHs, recent evidence highlights that NH_2 might react directly with soot particles, competing with C_2H_2 for active surface sites and thereby reducing HACA-mediated surface growth [17]. Incorporating these interactions was shown to be critical for accurately predicting both soot volume fraction and mean particle diameter. These findings underscore the need to consider nitrogen–soot surface chemistry, in addition to gas-phase N–PAH interactions, when interpreting soot suppression in NH_3-doped flames.

In this work, the contribution of NH_2 radical reacting with PAHs and soot particles is explored using a detailed kinetic model. The model adopted is based on a hierarchical and modular approach and accounts for i) C_0-C_4 and NH_3 chemistry, including interactions between small hydrocarbons and N-containing species, ii) gas-phase aromatic chemistry up to 5-ring PAHs and iii) detailed soot chemistry based on a discrete sectional approach.

In Section 2 the overall kinetic model is presented, with a focus on the specific reaction classes introduced in this work to describe the interaction between NH_2 and gas- and condensed-phase aromatic species. Section 3 benchmarks the model predictive capabilities against a wide range of measurements of soot volume fraction, average particle size [7,8] and particle size distribution [9] in laminar ethylene/ammonia flames in counterflow and premixed burner-stabilized stagnation configurations. Kinetic analyses are here performed to quantitatively assess the contribution of reactions between N-containing species and hydrocarbons on soot formation. However, in order to validate the present model, reliable experimental data on N-containing hydrocarbons, either HCN or N-PAHs, are needed to critically narrow down and discern the analysis of the actual pathways controlling soot formation in the presence of ammonia.

2. Kinetic model

A detailed kinetic model for the formation and oxidation of carbonaceous nanoparticles is used to evaluate the impact of ammonia on soot reduction in various ammonia/ethylene laminar flames. Particle reactivity, nanostructure, and morphology are described using the discrete sectional approach. Large-PAH and soot particles are discretized in lumped pseudo-species, named BINs, with a spacing factor of 2 in the number of C-atoms between adjacent sections. For each BIN, up to 3 different H/C ratios are considered. BIN1-4 represent large gas-phase PAH, from 20 to 160C-atoms. Recent theoretical calculations [18] suggest that large aromatic structures with >100 C-atoms behave as persistent, resonance-stabilized radicals. This assumption is adopted in the present model. BIN5-25 s represent soot particles larger than 2 nm, categorized as i) amorphous, liquid-like spherical particles; ii) solid primary particles with a more ordered internal nanostructure than their liquid-like counterparts; and iii) fractal aggregates composed of solid primary particles with a fractal dimension of $D_f = 1.8$. A detailed description of the different classification of the BINs adopted in the model can be found in previous works [19,20]. Seven main reaction classes are further considered to describe soot reactivity: inception, surface growth, carbonization, dehydrogenation, coalescence, aggregation and oxidation. Reference rate parameters of chemical pathways are taken from the analogy with gas-phase kinetics of aromatic species [21–23]. As regards physical pathways, instead, the size, temperature and H/C ratio dependent collision efficiency proposed by Pejpichestakul et al. [24] is adopted for aggregation reactions, while coalescence and carbonization rates were recently updated based the volume ratio of the colliding entities and particle size and H/C ratio, respectively, as described in [20].

In this work, two additional reaction classes, presented in Section 2.1, are included to account for amino radical (NH_2) interactions with both gas- and condensed- phases, namely, PAH and BIN species. The reference rate constants of the new classes listed in Table 1 are scaled according to the collision frequency (gas phase PAH/BIN) and particles surface areas (condensed phase) as explained in [25] and detailed in Section 2.1. Instead, HCN + PAH pathways were neglected since they only have a minor impact on soot formation [13]. Overall, ~ 700 elementary reactions that capture the interactions of the amino radicals with both large PAHs and BIN. Example of how the rate constants

Table 1
Reaction classes and related reference rate parameters introduced in the kinetic model.

Reaction class	Reference reaction	A [cm^3/mol/s]	E [cal/mol]
R1: NH_2 + PAH/BIN addition/recombination	$C_6H_5 + NH_2 => H + CYC_5H_5 + HCN$	$4.5x10^{13}$	4000/7000/10000*
R2f: H-abstraction by NH_2 (forward)	$C_6H_6 + NH_2 => C_6H_5 + NH_3$	$9.7x10^{10}$	12500
R2b: H-abstraction by NH_2 (backward)	$C_6H_5 + NH_3 => C_6H_6 + NH_2$	$9.6\ x10^{9}$	8000

* Activation energies used for NH_2 reactions with aromatic σ-, π-radicals and molecules, respectively.

change with sections size is shown in figure S5.

The kinetic model, developed using a hierarchical and modular approach, includes also $C_0 - C_4$ and NH_3 core chemistry, interactions between nitrogen-containing species and small hydrocarbons – including the $NH_3 + C_3H_3$ pathways reactions as proposed in [13], gas-phase aromatic chemistry up to five-ring PAH ($C_{18}H_{10}$ and $C_{18}H_{14}$), and soot kinetics [20,26,27]. Overall, the here update model accounts for 757 species and 131,146 reactions and it is available in the CHEMKIN format as supplementary material. Numerical simulations of the one-dimensional laminar flames in this study are conducted using the OpenSMOKE++ Suite [28]. The 1-D laminar flame solver incorporates mixture-average diffusion coefficients, the Soret effect, gas and soot radiation, and particle thermophoresis [29] within the species transport equations.

2.1. NH_2 reactions with PAH and soot

The present work introduces two main reaction classes listed in Table 1 alongside their respective reference reactions and rate parameters: R1) NH_2 addition/recombination and R2f) forward and R2b) backward H-abstraction by NH_2 onto from gas-phase aromatic species and soot particles. Specifically, for R1 a lumped pathway that ultimately leads to the removal of a C-atom from the aromatic structure as HCN is here considered following the theoretical investigation of Altarawneh et al. [30] and the experimental work by Colussi and Benson [31]. The latter investigated thermal decomposition of methylated anilines at high temperatures (T > 1200 K) and low pressures and found that HNC is released from the anilino radical, which decomposes following the N-C bond fission, in analogy to the ring contraction/CO elimination channel in phenoxy radical. HNC can then easily isomerize to HCN [30]. Fig. 1 depicts the mechanism of phenyl decomposition driven by NH_2 radical: aniline, formed by the recombination of the two radical reactants, releases an H-atom and subsequently decomposes to cyclopentadienyl radical and to either HCN or HNC [30].

In the present work, a first estimation of kinetic parameters of the global reaction depicted in Fig. 1 was carried out by applying a master equation-based lumping approach [32] with PES-derived rates from [30] to aniline decomposition into cyclopentadiene and HCN. The rate constants of the first reaction step, i.e., phenyl radical + NH_2, was estimated as 10^{14} cm^3/mol/s, in line with values for barrierless radical recombination reactions [13]. Then, the final rate parameters in Table 1 were approximated based on these first attempt parameters [30,32] and rate rules adopted for other reaction classes involving PAHs within the kinetic model [25]. Nevertheless, theoretical studies are needed to assess the quality of these assumptions. Instead, the reference kinetics for H-abstraction reactions by NH_2 (R2f and R2b) were taken from [30].

The pre-exponential factors, A_{ref}, proposed in Table 1 are then scaled for each section of the present sectional model according to the collision frequency, C_f, for large PAH:

$$A_{BIN} = A_{ref} \frac{C_f}{C_{f,ref}} \tag{1}$$

where, C_f is the collision frequency as defined in [33], and $C_{f,ref} = 2.26 \times 10^{-17}\sqrt{T}$ m^3/s refers to the collision frequency between phenyl and amino radicals. The pre-exponential factor of condensed phase reactions is instead scaled according to surface area and hydrogenation level as follows:

$$A_{BIN} = A_{ref}\left(1 + n_p \frac{d_p^2}{d_{p,ref}^2} \frac{H}{C}\right) \tag{2}$$

where n_p is the number of primary particles, d_p is the primary particle diameter, $d_{p,ref}$ is the reference primary particle diameter (2 nm) and H/C is the ration between hydrogen and carbon atom. The mechanism of NH_2-driven carbon loss in large PAH radicals/soot nanoparticles is shown Fig. S6.

Fig. 2 shows the reference rate constants adopted in the present model for R1 and R2. In Figs. 2a, R1 is compared with the recombination reaction rate constant calculated by Wang et al. [13] for $C_6H_5 + NH_2 => C_6H_5NH_2$. While the latter is barrierless, an activation energy of 4 kcal/mol is considered for the global reaction R1 in analogy with the rate constants for PAH oxidation by OH adopted in the present model [25], which is also in line with the slower subsequent elementary steps (see Fig. 1) leading to HCN elimination. For NH_2 addition/recombination reactions with aromatic molecules (C_6H_6) and π-radicals (e.g., benzyl C_7H_7), the activation energies are increased by 3 kcal/mol and 6 kcal/mol, respectively, consistent with other PAH reaction classes in the gas-phase model [23]. Fig. 2b shows that the reference rate constant adopted for R1 lies between the ones considered in the kinetic model for large PAH oxidation by OH (yellow dot-broken line) and O_2 (green dot-broken line), i.e., the main oxidizing species for PAHs and soot particles [25].

To quantify the impact of uncertainties in the estimated R1 rate constant, we performed a brute-force sensitivity analysis in flame F9 (20 % NH_3), perturbing the pre-exponential Arrhenius parameter independently by × 10 and ÷10. $A/10$ leads to an overprediction of peak SVF by a factor of around 4.5, whereas $A \times 10$ suppresses completely soot formation. Benzene and $C_{16}H_{10}$ mirror these trends, indicating that the R1 rate constant is a leading source of uncertainty for both PAH and soot predictions under NH_3 blending (see Figs. S2–S3). These findings motivate future kinetic studies to derive more accurate kinetic parameters for R1.

Finally, reaction class R2 contributes negligibly under the present conditions; however, it is retained for completeness of the kinetic mechanism. As illustrated in Fig. S4 (SI), which shows forward and reverse rates for a representative NH_2-mediated H-abstraction from benzene (C_6H_6), the reaction proceeds primarily in the reverse direction up to roughly 950 K. At higher temperatures, the forward reaction activates, yielding PAH radicals and NH_3. Therefore, although R2 remains globally weak, it acts mainly in the forward direction in the hottest regions of the flame.

3. Results and discussion

15 laminar ethylene/ammonia flames, in both counterflow and premixed burner-stabilized stagnation configurations, are here investigated. Their operating conditions are summarized in Table 2.

The first set of experimental data analyzed (flames F1–F9 in Table 2) are soot volume fraction (f_v) profiles measured by Bennett et al. [7] (F1-4, Table 2) and Zhou et al. [8] (F5-9, Table 2) in ammonia/ethylene counterflow flames and displayed in Figs. 3a and 3b respectively.

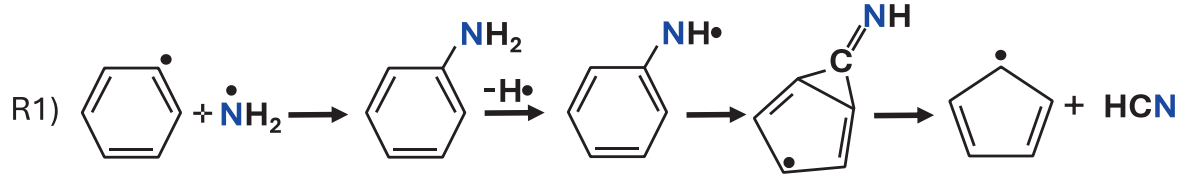

Fig. 1. Decomposition mechanism of phenyl radical reacting with NH_2 radical.

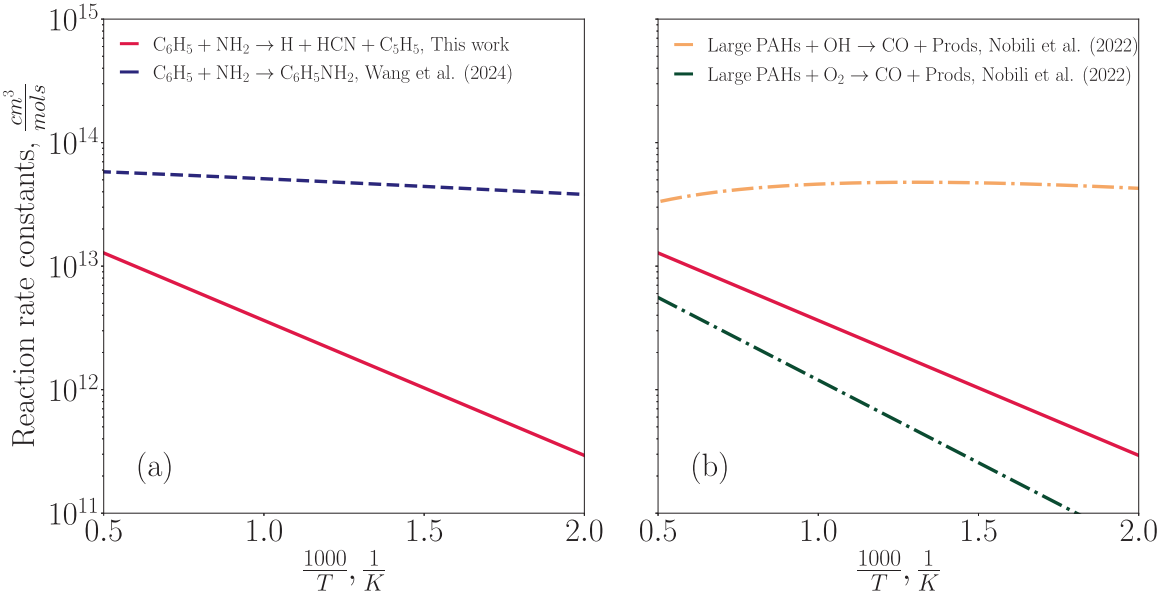

Fig. 2. Reference rate constant for R1 (solid lines) compared with kinetics from literature (a, broken lines [13]) and with reference rate constant for large PAHs and soot oxidation reaction class (b, dot-broken lines [25]).

Table 2
Operating conditions of laminar ammonia/ethylene flames investigated in this work.

Configuration	Flame	x_{NH3}	x_{C2H4}	T_{max} [K]	Z_{st}^a	K_G [s^{-1}]^b	L [mm]
Counterflow	F1	0.00	0.75	2232	0.0968	41	7.35
	F2	0.06	0.75	2412	0.0964	41	7.35
	F3	0.125	0.75	2247	0.957	41	7.35
	F4	0.25	0.75	2256	0.939	41	7.35
	F5	0.00	1.0	2261	0.06	101	8.0
	F6	0.05	0.95	2258	0.06	101	8.0
	F7	0.10	0.90	2258	0.06	100	8.0
	F8	0.15	0.85	2257	0.06	100	8.0
	F9	0.20	0.80	2254	0.06	100	8.0
					ϕ^c	V_0 [cm/s]^d	
Premixed BSS	F10	0.0000	0.163	1859	2.063	8.0	5
	F11	0.0163	0.163	1852	2.183	8.0	5
	F12	0.0326	0.163	1849	2.304	8.0	5
	F13	0.0000	0.163	1859	2.063	8.0	10
	F14	0.0163	0.163	1852	2.183	8.0	10
	F15	0.0326	0.163	1849	2.304	8.0	10

[a]Stoichiometric mixture fraction [b]Global strain rate. [c]Equivalence ratio. [d]Cold gas velocity.

In Fig. 3a, simulated counterflow flames (lines) with ammonia molar content varying from 0 to 25 % substituting the inert gas (argon, Ar) and fixed ethylene mole fraction of $x_{C2H4} = 0.75$, are benchmarked against soot volume fraction measurements (symbols, [7]) obtained by planar laser induced incandescence, PLII, with an uncertainty up to 50 % for large particles ($d_p > 50$ nm) [34]. Fig. 3b instead the shows results of simulations of Zhou et al. [8] counterflow flames where ammonia mole fraction is increased by 0.05 up to a maximum value of 0.20 and substitutes ethylene, compared with measurements by laser extinction and scattering technique. Fig. 3 demonstrates that the current model underestimates soot formation by factors of 4 and 1.8 for ammonia addition and substitution, respectively.

However, it is worth noting that the kinetic model adopted here has been largely validated against 30 laminar counterflow neat ethylene flames and it was proven to be on par with most of the measured peak f_v in the order of 1 ppm with discrepancies below a factor of 2 [20], in line with results in Fig. 3b. Because the F1 and F5 flame conditions are similar, the model produces similar outputs for both cases. The ~1.8 difference between our model and the experimental data [8] is consistent with previous validation [20] and is within the uncertainty of the model and laser diagnostics. In this regard, both datasets assume the same constant complex refractive index and use a wavelength-independent absorption function, $E(m) = 0.29$. However, the relative reduction of soot content with ammonia addition, which is the scope of this work, is not affected by these systemic uncertainties. In this regard, the present kinetic model shows that soot volume fraction peak is linearly reduced with ammonia increasing content with a reduction up to around 88 % for 25 % ammonia addition, perfectly on par with experimental data that display an 87 % reduction [7]. Therefore, accounting for NH_2 recombination and abstraction reactions in the condensed phase is fundamental to quantitatively describe NH_3 inhibiting effect on soot formation to the best of our knowledge. Indeed, neglecting cross reactions would lead to an overestimation by a factor of about 2 of the peak soot volume fractions in F4 and F9 (see Fig. S1 in supplementary material). Together with soot volume fraction, key morphological soot properties such as the evolution of average particle size (D_{63}) are here

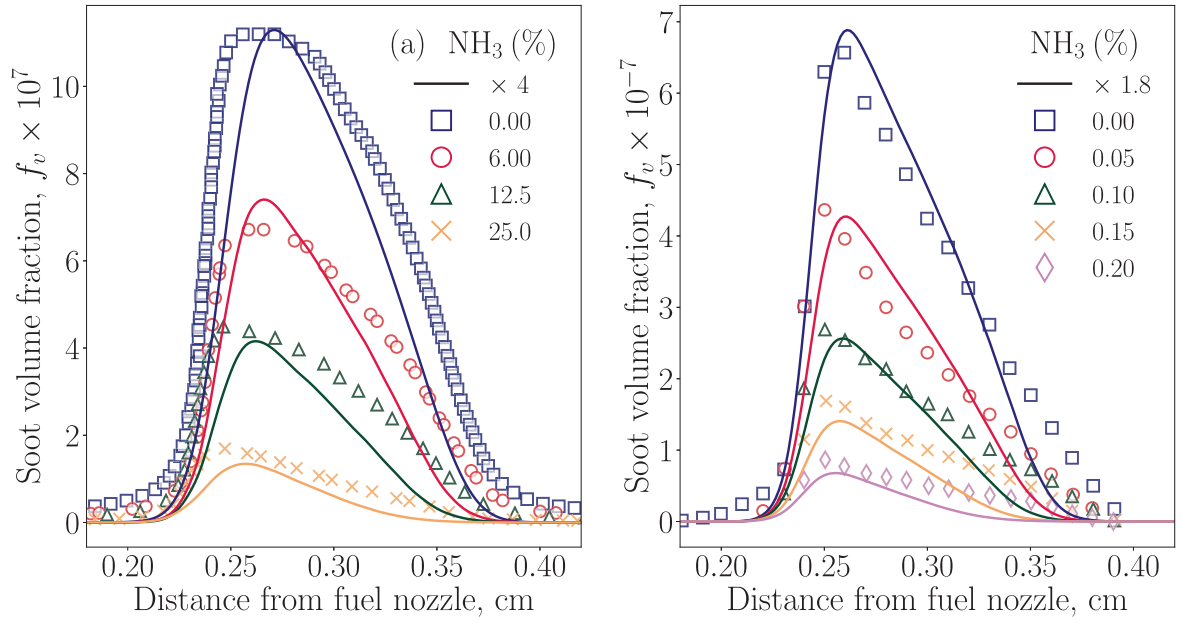

Fig. 3. Soot volume fraction, f_v, profiles measured (symbols [7,8]) and simulated (lines, this work) in a) F1-F4, [7] and b) F5-F9, [8] flames.

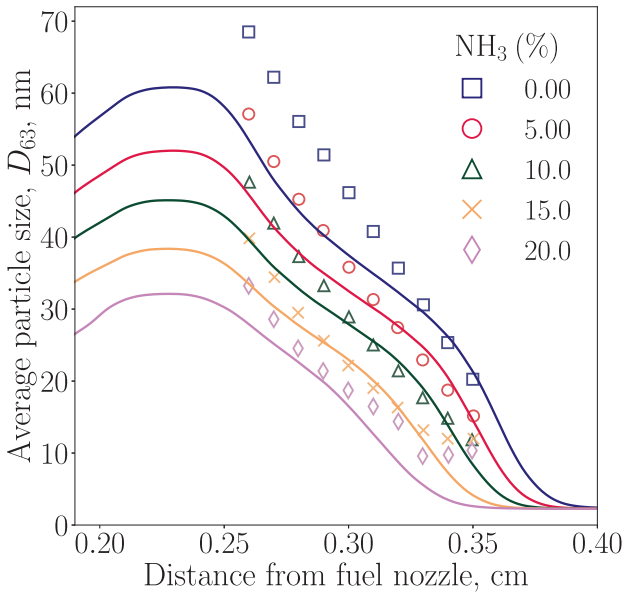

Fig. 4. Average particle size diameter profiles measured (symbols, [8]) and predicted (lines) in F5-F9 flames.

derived with the sectional model and compared to PLI measurements [8] in Fig. 4 for flames F5-F9. The model accurately predicts the decrease in D_{63} with NH_3 substitution along the entire axial coordinate, showing near-perfect agreement near the oxidizer side where particles form.

Fig. 5 shows the evolution of particle size distribution (PSD) (a,b) as well as soot volume fraction (c) evolution in laminar premixed burner-stabilized stagnation (BSS) $C_2H_4/NH_3/O_2/Ar$ flames experimentally studied by Shao et al. [9] (F10-F15 flames in Table 2) as a function of ammonia addition and distance from the burner H_p, i.e., residence time. PSD measurements are carried out by scanning mobility particle sizer consisting of a neutralizer, a nano-differential mobility analyser and an ultrafine condensation particle counter [9]. Here, ammonia molar content of 1.16 % (red line) and 3.26 % (green line) is added to ethylene and compared with pure C_2H_4 flames (blue lines). As already discussed in [20], the present sectional model reproduces reasonably the measured evolution of the soot volume fraction for the pure ethylene flame, F10, (Fig. 5c), as well as the trends observed for the PSD from $H_p = 5$ mm (Fig. 5a) to $H_p = 10$ mm (Fig. 5b), moving from a unimodal to a bimodal distribution. With increasing content of ammonia, at $H_p = 5$ mm a lower number of small nanoparticles (<6 nm) is generated, in perfect agreement with data, indicating that ammonia inhibits soot inception. At $H_p = 10$ cm, greater deviations between experimental data and simulations are observed (Fig. 5b). Specifically, in the NH_3-doped F14-F15 flames, measurements reveal a clear bimodal distribution with the PSD throat shifting towards larger diameters (~5–7 nm) compared to the pure ethylene case.

The present model predicts a unimodal distribution for NH_3-containing flames, overestimating particles formation for small sized particles ($d_p < 10$ nm) while the ammonia effect on the coagulation mode, i.e., larger particles, is well described by the present model. However, the model's inability to capture the observed bimodal evolution of the PSD suggests that NH_2 oxidation pathways remain insufficiently described, and that their coupling to soot inception and growth must be clarified to assess their impact on soot morphology and particle size. Moreover, the scaling law used in the discrete sectional model (i.e., BIN + NH_2 rate constants proportional to BIN surface area and hydrogenation level) fails to capture the NH_3-induced inhibition of soot formation, biasing growth in the smallest sections and damping the emergence of a bimodal PSD. In line with these deviations, the resulting soot volume fraction in ammonia-blended premixed flames is well reproduced only in the inception zone (low residence time, $H_p = 5$ mm), while discrepancies increase at longer residence times and higher ammonia contents.

Beyond soot properties (f_v, D_{63} and PSD), we qualitatively assess gas-phase aromatic formation in NH_3/C_2H_4 counterflow flames (F1-F4) against the PLIF measurements of Bennett et al. [7]. Different PAHs at four given signal intensities are compared to the model predictions, in Fig. 6, where PAHs are grouped according to a species-to-wavelength mapping (Table S1, detailed approach in [35]). The 350, 400, 450, and 500 nm wavelength correspond to 1-, 2-, 3-, and 4-ring PAHs, respectively. Fig. 6 reports peak PLIF intensities and peak simulated mole fractions, each normalized by the F1 peak values. At 350 nm, the measured PLIF signal is only weakly affected by NH_3 addition, which

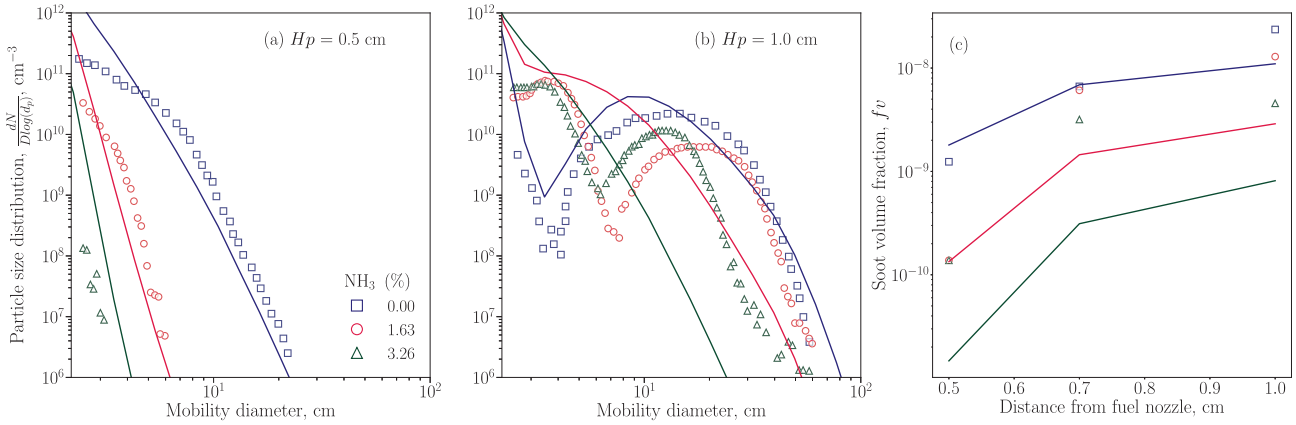

Fig. 5. Measured [9] (symbols) and predicted (lines) particle size distribution (PSD) at a) H_p = 5 mm and b) H_p = 10 mm and soot volume fraction c) in F10-F15 flames.

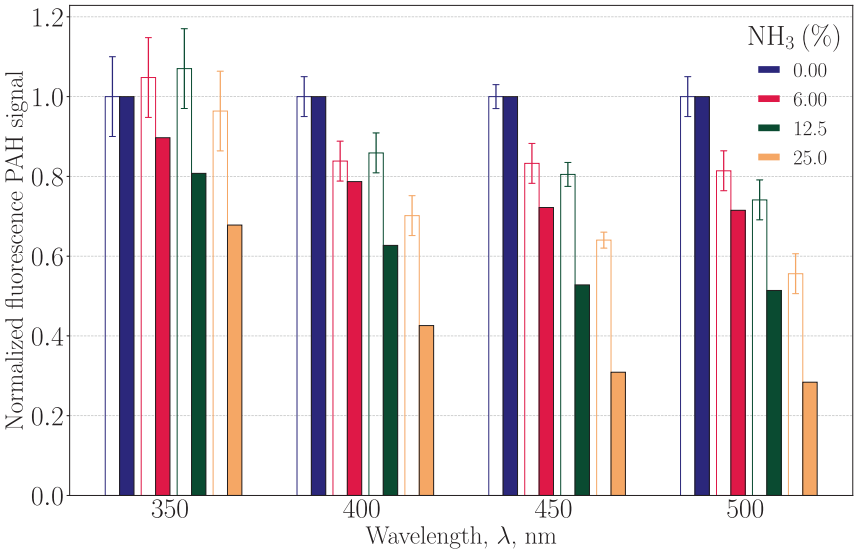

Fig. 6. Comparison between measured peak PAH PLIF signals (empty bar, [7]) and simulated peak mole fraction of gas-phase aromatic species in F1-F4 flames (filled bar). Values normalized with respect to F1.

would suggest limited experimental sensitivity of early soot precursors (e.g., 1-ring PAHs such as benzene) to nitrogen chemistry. However, this apparent insensitivity should be interpreted with caution. First, diagnostics sensitivity plays a role: PLIF yields depend on excitation/emission spectra, quenching, and filter bandwidths, and species such as NH_3, H_2O, and HCN can modify fluorescence lifetimes and effective quantum yields.

These effects can flatten the observed NH_3 dependence of the 350 nm signal. Second, uncertainties in LIF cross-sections are larger at 350 nm, such that the band may also include overlapping contributions from larger aromatics. In contrast with the experimental trend at 350 nm, the model predicts a decrease in benzene and other early soot precursors with increasing ammonia content, primarily driven by NH_2 recombination pathways. This behavior is consistent with previous experimental and theoretical studies [11,14,17], which attribute soot inhibition by ammonia to gas-phase reactions that consume soot precursors. For $\lambda \geq$ 400 nm, the model reproduces the experimental trends more directly: the PAH-related signal decreases approximately linearly with NH_3 addition, supporting the interpretation that ammonia suppresses the growth of larger, condensed-phase PAHs. For example, the simulated peak mole fraction of 4-ring PAHs (500 nm) decreases nearly linearly with increasing ammonia content, highlighting in particular the role of R1 (Fig. 7).

Mechanistically, NH_2 radicals interact with early soot precursors such as benzene and pyrene. Fig. 7 shows production/consumption rate profile along the axial coordinate for F1 (0 % NH_3 – left) and F4 (25 % NH_3 – right) considering only decomposition and growth reactions. In the pure ethylene case, F1, benzene forms chiefly via propargyl self-recombination and the HACA mechanism, while pyrene growth is dominated by HACA. With ammonia addition, NH_2-driven decomposition pathways become the principal sinks for both benzene and pyrene, yielding HCN and ultimately reducing soot formation. It is worth mentioning that the temperature profiles calculated in this region for F1 and F4 flames almost overlap. Fig. 8 reports the molar fractions profiles of a) HCN and b) NH_2 for flames F1 (0 % NH_3) –F2 (6 % NH_3) –F3 (12.5 % NH_3) and F4 (25 % NH_3). Although experimental data are not available in the literature to validate the resulting profiles, as expected, both HCN and NH_2 profiles increase with increasing ammonia content. Interestingly, the increase of NH_2 mole fraction, Fig. 8c, strongly resemble the decrease of soot volume fraction (Fig. 3a) moving from F1 to F4, which may support the primary role played by amino radicals in suppressing soot formation in NH_3-doped flames. Indeed, while soot

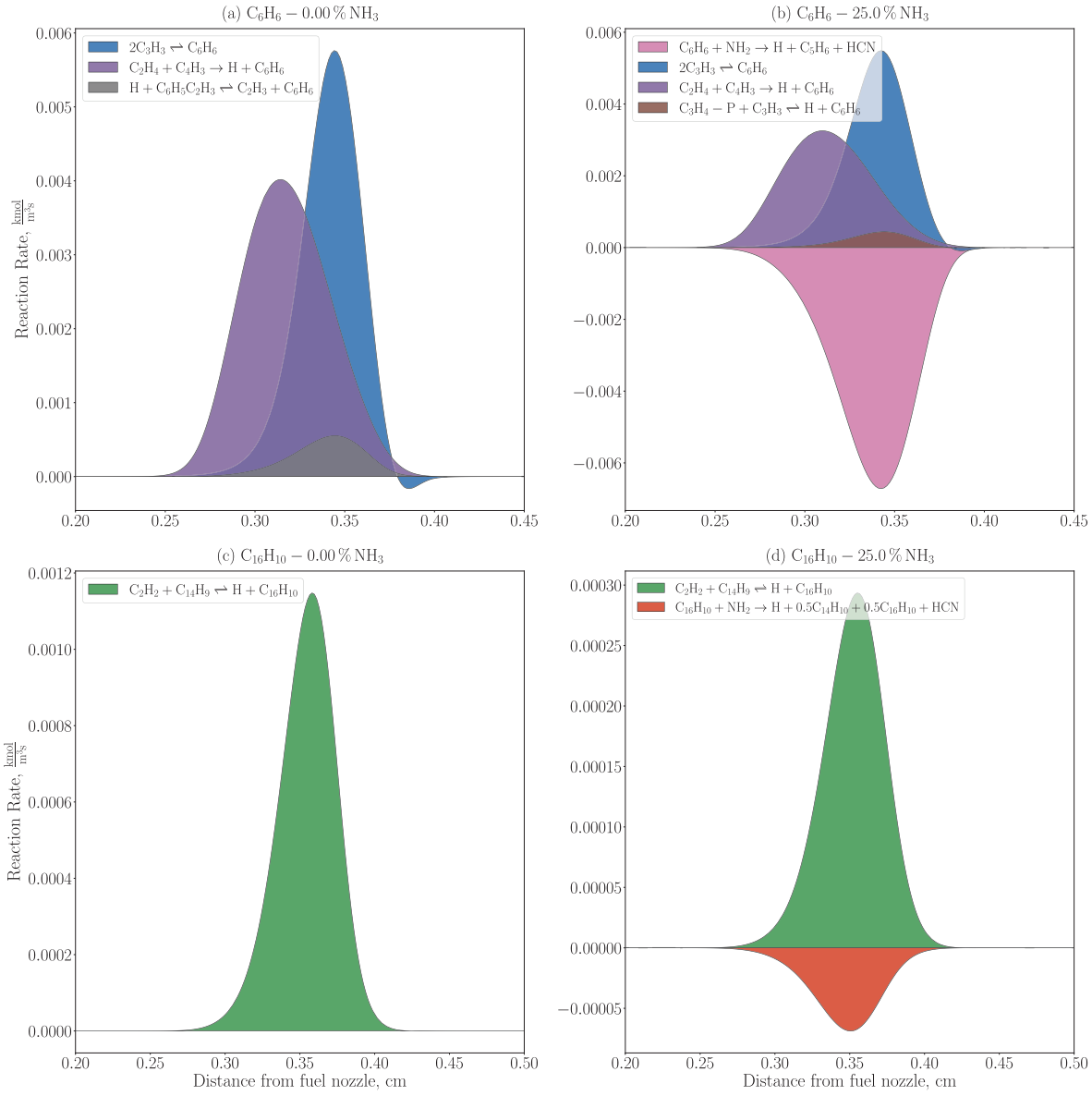

Fig. 7. A, b) benzene and c, d) pyrene production/consumption rate profiles along the axial flame coordinate in f1 (pure c_2H_4, top panels) and F4 (25 % NH_3 addition, bottom panels).

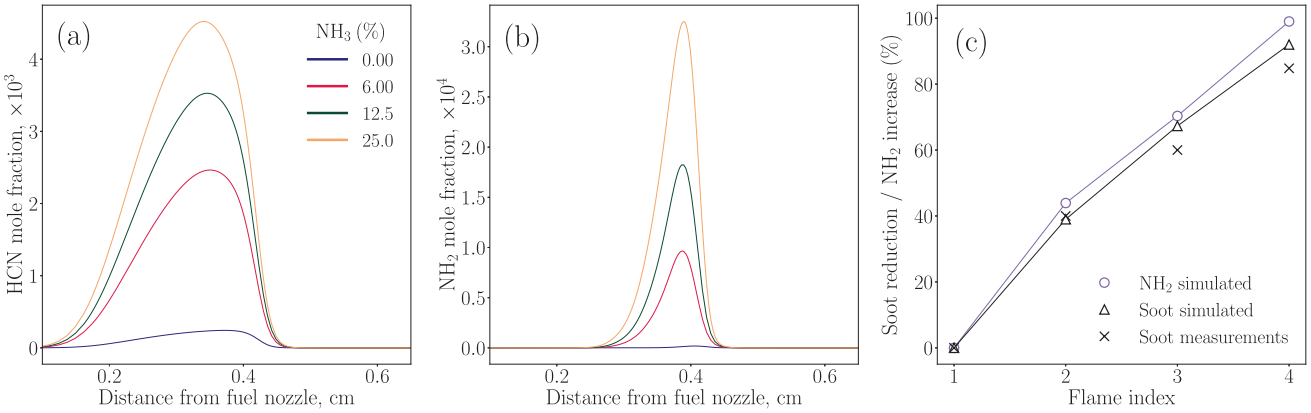

Fig. 8. Simulated mole fraction profiles of a) HCN and b) NH_2 and c) relative simulated soot volume fraction peak reduction compared to soot measurements and to computed NH_2 molar fraction peak increase in F1-F4 flames.

volume fraction peak displays a reduction of around 87 % for F4 with respect of F1, HCN and NH_2 molar fraction peaks face a reduction of 95 % and 98 % respectively, varying NH_3 content between 25 % and 0 %.

Finally, it is worth mentioning that among the alternative pathways summarized in Section 1 and proposed in the literature as responsible of soot reduction due to NH_3-doping in hydrocarbon flames, both the HCN + PAH pathways and the $C_2H_2 + N <=> HCN + CH$ reaction proposed in [11] and [15] respectively, were tested. However, the impact of both reaction pathways on soot reduction is found to be negligible when included in the present kinetic model.

4. Conclusions

This study investigates the effect of ammonia on reducing soot formation in ethylene laminar flames using a semi-detailed kinetic model. Specifically, the study numerically explores the impact of NH_2 radical by incorporating its interactions with gas-phase aromatic species and soot particles into the adopted model. In this regard, due to the lack of theoretical studies dedicated to these decomposition pathways, tentative reference reaction rate constants have been proposed and discussed. Given the limited data available in the literature, it is proposed that NH_2 drives the decomposition of aromatic species through addition and abstraction reactions. For the first reaction class, it has been considered that the C-atom removal from the aromatic structure occurs through the release of HCN. The model here presented is tested against data of soot volume fraction (f_v) profiles in two series of counterflow flames. A maximum model overestimation of f_v peak by factor of 4 has been obtained, with very good predictions of the trend in the measured soot reduction in the case of both ammonia addition and substitution to ethylene. The model can also satisfactorily predict key morphological soot properties such as the evolution of the average particle size (D_{63}) in counterflow flames and of the particle size distribution (PSD) in premixed burner stabilized stagnation flames at $H_p = 5$ mm for different NH_3 contents. However, it was shown that the model cannot reproduce the bimodal distribution of the PSD when ammonia is added to ethylene at $H_p = 10$ mm. Furthermore, measured peak PAH PLIF signals and simulated peak mole fraction have been qualitatively compared. In both measurements and simulations, it has been observed a more pronounced reduction of large aromatic species ($\geq$2-ring PAHs). Future experimental studies quantifying nitrogen-containing hydrocarbons in laminar flames, alongside theoretical investigations of NH_2 radicals' role in suppressing aromatic growth, are crucial for validating this kinetic modelling study and refining the understanding of pathways governing soot formation in ammonia-containing flames.

CRediT authorship contribution statement

P. Crepaldi: Writing – original draft, Validation, Software, Project administration, Methodology, Investigation, Formal analysis, Data curation, Conceptualization. **A. Nobili:** Writing – review & editing, Writing – original draft, Visualization, Validation, Supervision, Project administration, Methodology, Investigation, Formal analysis, Data curation, Conceptualization. **T. Dinelli:** Writing – review & editing, Investigation, Formal analysis, Data curation, Conceptualization. **L. Pratali Maffei:** Writing – review & editing, Supervision, Methodology, Formal analysis, Data curation, Conceptualization. **A. Cuoci:** Writing – review & editing, Methodology, Data curation. **T. Faravelli:** Writing – review & editing, Visualization, Validation, Supervision, Resources, Project administration, Methodology, Investigation, Funding acquisition, Formal analysis, Conceptualization.

Declaration of competing interest

The authors declare that they have no known competing financial interests or personal relationships that could have appeared to influence the work reported in this paper.

Appendix A. Supplementary data

Supplementary data to this article can be found online at https://doi.org/10.1016/j.fuel.2025.137695.

Data availability

Kinetic model is provided in the supplementary material.

References

[1] Valera-Medina A, Xiao H, Owen-Jones M, David WIF, Bowen PJ. Ammonia for power. Prog Energy Combust Sci 2018;69:63–102.
[2] Kobayashi H, Hayakawa A, Somarathne KDKA, Okafor EC. Science and technology of ammonia combustion. Proc Comb Inst 2019;37:109–33.
[3] Christensen CH, Johannessen T, Sørensen RZ, Nørskov JK. Towards an ammonia-mediated hydrogen economy? Catal Today 2006;111:140–4.
[4] He X, Shu B, Nascimento D, Moshammer K, Costa M, Fernandes RX. Auto-ignition kinetics of ammonia and ammonia/hydrogen mixtures at intermediate temperatures and high pressures. Combust Flame 2019;206:189–200.
[5] Ramanathan V, Carmichael G. Global and regional climate changes due to black carbon. Nat Geosci 2008;1(4):221–7.
[6] Bach PB, Kelley MJ, Tate RC, McCrory DC. Screening for lung cancer: a review of the current literature. Chest 2003;123:72S–82S.
[7] Bennett AM, Liu P, Li Z, Kharbatia NM, Boyette W, Masri AR, et al. Soot formation in laminar flames of ethylene/ammonia. Combust Flame 2020;220:210–8.
[8] Zhou M, Yan F, Ma L, Jiang P, Wang Y, Ho Chung S. Chemical speciation and soot measurements in laminar counterflow diffusion flames of ethylene and ammonia mixtures. Fuel 2022;308.
[9] Shao C, Campuzano F, Zhai Y, Wang H, Zhang W, Sarathy M. Effects of ammonia addition on soot formation in ethylene laminar premixed flames. Combust Flame 2022;235.
[10] Steinmetz SA, Ahmed HA, Boyette WR, Dunn MJ, Roberts WL, Masri AR. Effects of ammonia and hydrogen on the sooting characteristics of laminar coflow flames of ethylene and methane. Fuel 2022;307.
[11] Liu Y, Cheng X, Li Y, Qiu L, Wang X, Xu Y. Effects of ammonia addition on soot formation in ethylene laminar diffusion flames. Fuel 2021;292:120416.
[12] Montgomery MJ, Kwon H, Dreyer JAH, Xuan Y, McEnally CS, Pfefferle LD. Effect of ammonia addition on suppressing soot formation in methane co-flow diffusion flames. Proc Comb Inst 2021;38:2497–505.
[13] Wang Q, Wang T, Sarathy SM. A PAH growth mechanism for nitrogen-containing aromatics in ammonia-doped hydrocarbon flames. Proc Comb Inst 2024;40.
[14] Tang X, Xing J, Luo K, Fan J, Gu M. Numerical study on soot formation in ammonia/ethylene laminar counterflow diffusion flame. Fuel 2024;371:131965.
[15] Ao C, Yan J, Yan T, Zhang L, Wang P. A theoretical and modeling study of nitrogen chemistry in polycyclic aromatic hydrocarbons growth process. Combust Flame 2024;259:113183.
[16] Liu Y, Xu Y, Zhang K, Zhang P, Cheng X. Effects of ammonia addition on soot formation in ethylene laminar diffusion flames. Part 3. The morphology and nanostructure of soot particles. Fuel 2023;332:126082.
[17] Guo J, Chu C, Wang Q, Liu P, Aydin FY, Quadarella E, Sarathy SM, Roberts WL, Im HG. Chemical suppressive effect of ammonia addition on soot formation in laminar diffusion flames. Proc Comb Inst 2024;40.
[18] Nobili A, Pratali Maffei L, Baggioli A, Pelucchi M, Cuoci A, Cavallotti C, et al. On the radical behavior of large polycyclic aromatic hydrocarbons in soot formation and oxidation. Combust Flame 2022;235:111692.
[19] Saggese C, Ferrario S, Camacho J, Cuoci A, Frassoldati A, Ranzi E, et al. Kinetic modeling of particle size distribution of soot in a premixed burner-stabilized stagnation ethylene flame. Combust Flame 2015;162:3356–69.
[20] Nobili A, Fanari N, Dinelli T, Cipriano E, Cuoci A, Pelucchi M, et al. Kinetic modeling of carbonaceous particle morphology, polydispersity and nanostructure through the discrete sectional approach. Combust Flame 269 2024.
[21] Pratali Maffei L, Pelucchi M, Cavallotti C, Bertolino A, Faravelli T. Master equation lumping for multi-well potential energy surfaces: a bridge between ab initio based rate constant calculations and large kinetic mechanisms. Chem Eng J 2021;422.
[22] Pelucchi M, Cavallotti C, Faravelli T, Klippenstein SJ. H-Abstraction reactions by OH, HO2, O, O2 and benzyl radical addition to O2 and their implications for kinetic modelling of toluene oxidation. PCCP 2018;20:10607–27.
[23] Nobili A, Veltri M, D'Andria M, Pelucchi M, Faravelli T, Mehl M. A kinetic study on the blending behavior of sustainable and conventional aviation fuels: Soot formation processes. Proc Comb Inst 2024;40.
[24] Pejpichestakul W, Frassoldati A, Parente A, Faravelli T. Kinetic modeling of soot formation in premixed burner-stabilized stagnation ethylene flames at heavily sooting condition. Fuel 2018;234:199–206.
[25] Nobili A, Pejpichestakul W, Pelucchi M, Cuoci A, Cavallotti C, Faravelli T. Modeling soot particles as stable radicals: a chemical kinetic study on formation and oxidation. Part II. Soot oxidation in flow reactors and laminar flames. Combust Flame 2022;243.
[26] Arunthanayothin S, Stagni A, Song Y, Herbinet O, Faravelli T, Battin-Leclerc F. Ammonia–methane interaction in jet-stirred and flow reactors: an experimental and kinetic modeling study. Proc Comb Inst 2021;38:345–53.

[27] Stagni A, Cavallotti C, Arunthanayothin S, Song Y, Herbinet O, Battin-Leclerc F, et al. An experimental, theoretical and kinetic-modeling study of the gas-phase oxidation of ammonia. React Chem Eng 2020;5:696–711.
[28] Cuoci A, Frassoldati A, Faravelli T, Ranzi E. OpenSMOKE++, An object-oriented framework for the numerical modeling of reactive systems with detailed kinetic mechanisms. Comput Phys Commun 2015;192:237–64.
[29] Zheng D, Nobili A, Cuoci A, Pelucchi M, Hui X, Faravelli T. Soot formation from n-heptane counterflow diffusion flames: two-dimensional and oxygen effects. Combust Flame 2023;258.
[30] Altarawneh IS, Altarawneh M, Rawadieh SE, Almatarneh MH, Shiroudi A, El-Nahas AM. Updated yields of nitrogenated species in flames of ammonia/benzene via introducing an aniline sub-mechanism. Combust Flame 2021;228:433–42.
[31] Colussi AJ, Benson SW. Very-low-pressure pyrolysis of N-methyl aniline and N,N-dimethyl aniline. Enthalpy of formation of the anilino and N-methyl anilino radicals. Int J Chem Kinet 1978;10:1139–49.
[32] Pratali Maffei L, Pelucchi M, Cavallotti C, Bertolino A, Faravelli T. Master equation lumping for multi-well potential energy surfaces: a bridge between ab initio based rate constant calculations and large kinetic mechanisms. Chem Eng J 2021;422:129954.
[33] Fuchs NA, Daisley RE, Fuchs M, Davies CN, Straumanis ME. The mechanics of aerosols. Phys Today 1965;18:73.
[34] Bennett A, Amin HMF, Cenker E, Roberts WL. Measurements of pressure effects on PAH distribution and 2D soot volume fraction diagnostics in a laminar non-premixed coflow flame. Energy Fuels 2018;32:10974–83.
[35] Zheng D, Nobili A, Cuoci A, Pelucchi M, Hui X, Faravelli T. Soot formation from n-heptane counterflow diffusion flames: two-dimensional and oxygen effects. Combust Flame 2023;258:112441.